

# Renormalization group analysis of the 2D Hubbard model

Christoph J. Halboth and Walter Metzner

*Institut für Theoretische Physik C, Technische Hochschule Aachen  
Templergraben 55, D-52056 Aachen, Germany*

(September 5, 2018)

Salmhofer [Commun. Math. Phys. **194**, 249 (1998)] has recently developed a new renormalization group method for interacting Fermi systems, where the complete flow from the bare action of a microscopic model to the effective low-energy action, as a function of a continuously decreasing infrared cutoff, is given by a differential flow equation which is local in the flow parameter. We apply this approach to the repulsive two-dimensional Hubbard model with nearest and next-nearest neighbor hopping amplitudes. The flow equation for the effective interaction is evaluated numerically on 1-loop level. The effective interactions diverge at a finite energy scale which is exponentially small for small bare interactions. To analyze the nature of the instabilities signalled by the diverging interactions we extend Salmhofers renormalization group for the calculation of susceptibilities. We compute the singlet superconducting susceptibilities for various pairing symmetries and also charge and spin density susceptibilities. Depending on the choice of the model parameters (hopping amplitudes, interaction strength and band-filling) we find commensurate and incommensurate antiferromagnetic instabilities or  $d$ -wave superconductivity as leading instability. We present the resulting phase diagram in the vicinity of half-filling and also results for the density dependence of the critical energy scale.

PACS: 71.10.Fd, 71.10.-w, 74.20.Mn

## I. INTRODUCTION

One of the striking aspects of the high-temperature superconducting cuprates is the sensitive dependence of their physical properties on the charge carrier concentration in the copper-oxide planes, which can be continuously varied by doping the inter-plane region. In the doping-temperature phase-diagram one generically finds an antiferromagnetic insulator and a superconducting phase with  $d$ -wave symmetry, with strongly doping dependent transition temperatures in each case [1].

The two-dimensional Hubbard model [2] is a promising prototype model for the electronic degrees of freedom in the copper-oxide planes. It has an antiferromagnetically ordered ground state at half-filling and is expected to become a  $d$ -wave superconductor at moderate doping away from half-filling [3].

Although the Coulomb interaction in the cuprates is certainly rather strong, there has been considerable recent interest in the *weak* coupling sector of the 2D Hubbard model. Besides the applicability of (semi-) analytical methods at weak coupling and the general experience that many strongly interacting systems are more or less continuously connected to corresponding weak coupling systems, a major reason for this interest is that even the weakly interacting 2D Hubbard model exhibits an extraordinarily rich behavior as a function of the carrier density and other model parameters. Conventional perturbation theory breaks down for densities close to half-filling, where numerous competing infrared divergences appear as a consequence of Fermi surface nesting and van Hove singularities. These divergencies can in principle be treated by suitable self-consistent resummations of perturbative contributions to all orders in the cou-

pling constant. Most notably the so-called fluctuation-exchange approximation [4] turned out to be able to describe various expected physical properties. However, a completely unbiased selection of Feynman diagrams that takes into account all possible particle-particle and particle-hole channels on equal footing would require at least the self-consistent summation of all parquet diagrams [5], which is still beyond present numerical possibilities for sufficiently large systems and low temperatures.

Renormalization group (RG) methods are presently the most promising and best controlled approach to low dimensional Fermi systems with competing singularities at weak coupling. Such methods have been developed long ago for one-dimensional systems where, combined with exact solutions of fixed point models, they have been a major source of physical insight [6,7]. Early RG studies of two-dimensional systems started with simple but ingenious scaling approaches to the 2D Hubbard model, very shortly after the discovery of high- $T_c$  superconductivity [8–10]. These studies focussed on dominant scattering processes between van Hove points in  $k$ -space, for which a small number of running couplings could be defined and computed on 1-loop level. Spin-density and superconducting instabilities were identified from divergencies of the corresponding correlation functions. Recently, the early scaling approaches have been revisited by various authors to extract further physical properties, such as a possible pinning of the Fermi level at the van Hove singularity [11], extended saddle points [11,12], and a possible gap formation on parts of the Fermi surface near the van Hove points [13]. Scaling theories with few running couplings have also been used to analyze instabilities associated with flat Fermi surface pieces [14,15] and inflection

points on the Fermi surface [16].

A major complication in two-dimensional systems compared to 1D is that the effective interactions cannot be parameterized accurately by a small number of running couplings, even if irrelevant momentum and energy dependences are neglected, since the tangential momentum dependence of effective interactions along the Fermi “surface” (a line in 2D) is strong and important in the low-energy limit. This has been demonstrated in particular in a 1-loop RG study for a model system with two parallel flat Fermi surface pieces [17]. In an impressive series of recent papers Zanchi and Schulz [18] have developed a new renormalization group approach for interacting Fermi systems, which is based on a flow equation derived by Polchinski [19] in the context of local quantum field theory. In this RG version the complete flow from the bare action of an arbitrary microscopic model to the effective low-energy action, as a function of a continuously decreasing infrared energy cutoff, is given by an exact differential flow equation. Zanchi and Schulz have applied this approach to the 2D Hubbard model (with nearest neighbor hopping) in a 1-loop approximation, with a discretized tangential momentum dependence of the effective 2-particle interaction. The presence of anti-ferromagnetism and *d*-wave superconductivity as major instabilities of the model close to half-filling was thereby confirmed.

The development of continuous renormalization group methods for interacting Fermi systems has made further progress with a most recent work by Salmhofer [20]. By expanding the effective action in Wick-ordered monomials instead of bare monomials he obtained an exact flow equation for the effective interactions with a particularly convenient structure: The  $\beta$ -function is bilinear in the effective interactions and *local* in the flow parameter, i.e. it does not depend on effective interactions at higher energy scales.

In this work we apply Salmhofer’s RG version to the two-dimensional Hubbard model with nearest and also next-nearest neighbor hopping amplitudes, concentrating on the most interesting electron density regime near half-filling. We evaluate the flow of effective (2-particle) interactions on 1-loop level, neglecting the irrelevant energy dependence and also the irrelevant normal momentum dependence, but keeping the important tangential momentum dependence. As in previous RG calculations, the effective interactions diverge at a finite energy scale, which is exponentially small for a small bare interaction. To analyze the physical nature of the instabilities signalled by the diverging interactions we extend Salmhofer’s RG version for the calculation of susceptibilities. We compute charge and spin susceptibilities and singlet superconducting susceptibilities for various pairing symmetries. Depending on the choice of the model parameters, hopping amplitudes, interaction strength and band-filling, we find commensurate or incommensurate antiferromagnetic instabilities or *d*-wave superconductivity as leading instability, in qualitative agreement with

previous calculations with other RG versions. We present the resulting phase diagram of the two-dimensional Hubbard model near half-filling and results showing how the critical energy scale decreases away from the half-filled perfect nesting case.

We finally note that powerful renormalization group techniques with a discrete successive reduction of the infrared cutoff have recently opened the way towards a rigorous non-perturbative control of interacting Fermi systems for sufficiently small yet finite coupling strength [21]. Significant rigorous results have already been derived for 2D systems [22]. These mathematical works show in particular that all weak coupling instabilities in interacting Fermi systems can be obtained systematically from a renormalization group analysis.

This article is organized as follows. In Section II we briefly review Salmhofer’s RG for general interacting Fermi systems, present the explicit flow equations for effective 2-particle interactions on 1-loop level, and also derive the flow equations for susceptibilities. In Section III we first discuss how the 1-loop flow equations are solved, and then present numerical results for the Hubbard model with a discussion of their physical content. Section IV closes the presentation with a short summary of major results and some ideas for further developments.

## II. RENORMALIZATION GROUP EQUATIONS

In this section we review Salmhofer’s renormalization group approach for general interacting Fermi systems, present the explicit flow equations for effective 2-particle interactions on 1-loop level, and finally derive 1-loop flow equations for several susceptibilities, which will later be used for our stability analysis of the 2D Hubbard model.

### A. Functional integral representation

We consider a system of interacting spin- $\frac{1}{2}$  fermions with a single particle basis given by states with a (crystal) momentum  $\mathbf{k}$ , a spin projection  $\sigma \in \{\uparrow, \downarrow\}$ , and a kinetic energy  $\epsilon_{\mathbf{k}}$ . The properties of the system are determined by an action

$$S[\psi, \bar{\psi}] = \sum_K (ik_0 - \xi_{\mathbf{k}}) \bar{\psi}_K \psi_K - V[\psi, \bar{\psi}] \quad (1)$$

where  $K = (k_0, \mathbf{k}, \sigma)$  is a multi-index containing the Matsubara frequency  $k_0$  in addition to the single particle quantum numbers;  $\bar{\psi}_K$  and  $\psi_K$  are Grassmann variables associated with creation and annihilation operators,  $\xi_{\mathbf{k}} = \epsilon_{\mathbf{k}} - \mu$  is the single-particle energy relative to the chemical potential, and  $V[\psi, \bar{\psi}]$  is an arbitrary many-body interaction. The non-interacting single-particle propagator of the system is given by

$$C(K) = \frac{1}{ik_0 - \xi_{\mathbf{k}}} \quad (2)$$

All connected Green functions can be obtained from the generating functional [23]

$$\mathcal{G}[\eta, \bar{\eta}] = \log \left\{ \int d\mu_C[\psi, \bar{\psi}] e^{-V[\psi, \bar{\psi}]} e^{(\bar{\psi}, \eta) + (\bar{\eta}, \psi)} \right\} \quad (3)$$

with the normalized Gaussian measure

$$d\mu_C[\psi, \bar{\psi}] = \prod_K d\psi_K d\bar{\psi}_K e^{(\bar{\psi}, C^{-1}\psi)} / \int \prod_K d\psi_K d\bar{\psi}_K e^{(\bar{\psi}, C^{-1}\psi)} \quad (4)$$

Here we have introduced the short-hand notation  $(\chi, \psi) = \sum_K \chi_K \psi_K$  and  $(C^{-1}\psi)_K = C^{-1}(K) \psi_K$  for arbitrary Grassmann variables  $\chi_K$  and  $\psi_K$ . Note the identity

$$\int d\mu_C[\psi, \bar{\psi}] e^{(\bar{\psi}, \eta) + (\bar{\eta}, \psi)} = e^{-(\bar{\eta}, C\eta)} \quad (5)$$

which implies that  $\mathcal{G}[\eta, \bar{\eta}] = -(\bar{\eta}, C\eta)$  in the non-interacting case  $V[\psi, \bar{\psi}] = 0$ . The connected  $m$ -particle Green functions are given by

$$\begin{aligned} G_m(K'_1, \dots, K'_m; K_1, \dots, K_m) &= \\ &= (-1)^m \langle \psi_{K'_1} \dots \psi_{K'_m} \bar{\psi}_{K_m} \dots \bar{\psi}_{K_1} \rangle_c \\ &= \frac{\partial^m}{\partial \bar{\eta}_{K'_1} \dots \partial \bar{\eta}_{K'_m}} \frac{\partial^m}{\partial \eta_{K_m} \dots \partial \eta_{K_1}} \mathcal{G}[\eta, \bar{\eta}] \Big|_{\eta=\bar{\eta}=0} \end{aligned} \quad (6)$$

where  $\langle \dots \rangle_c$  is the connected average of the product of Grassmann variables between the brackets.

The renormalization group equations are most conveniently formulated for another generating functional, the *effective interaction* [24]

$$\mathcal{V}[\chi, \bar{\chi}] = -\log \left\{ \int d\mu_C[\psi, \bar{\psi}] e^{-V[\psi+\chi, \bar{\psi}+\bar{\chi}]} \right\} \quad (7)$$

A simple substitution of variables yields the relation

$$-\mathcal{V}[\chi, \bar{\chi}] = (\bar{\eta}, C\eta) + \mathcal{G}[\eta, \bar{\eta}] \quad \text{where } \chi = C\eta, \bar{\chi} = C\bar{\eta} \quad (8)$$

where  $\dot{C}^\Lambda(K) = \partial C^\Lambda(K) / \partial \Lambda$ . With the initial condition

$$\mathcal{V}^{\Lambda_0}[\chi, \bar{\chi}] = V[\chi, \bar{\chi}] \quad (12)$$

this equation determines the flow of  $\mathcal{V}^\Lambda$  uniquely for all  $\Lambda < \Lambda_0$ . The initial value  $\Lambda_0$  must be chosen such that  $\Theta_>^\Lambda(K) = 0$  for all  $K$  and  $\Lambda > \Lambda_0$ . For the step function

Hence, functional derivatives of  $\mathcal{V}[\chi, \bar{\chi}]$  generate connected Green functions divided by  $C(K_1) \dots C(K_m) C(K'_1) \dots C(K'_m)$ , i.e. (non-interacting) propagators are amputated from external legs in the corresponding Feynman diagrams. The term  $(\bar{\eta}, C\eta)$  cancels the non-interacting part of  $\mathcal{G}[\bar{\eta}, \eta]$  such that  $\mathcal{V}[\chi, \bar{\chi}] = 0$  for  $V[\psi, \bar{\psi}] = 0$ . Hence, the non-interacting propagator is subtracted from the one-particle Green function generated by  $\mathcal{V}$ .

## B. Wick-ordered continuous RG

We now briefly review the derivation of a continuous renormalization group equation for Wick-ordered (amputated) Green functions, as first derived in the context of interacting Fermi systems by Salmhofer [20].

The original system is endowed with an infrared cutoff at an energy scale  $\Lambda > 0$  by replacing the bare propagator  $C(K)$  with

$$C^\Lambda(K) = \frac{\Theta_>^\Lambda(K)}{ik_0 - \xi_{\mathbf{k}}} \quad (9)$$

Here  $\Theta_>^\Lambda(K)$  is a function that vanishes for  $\sqrt{k_0^2 + \xi_{\mathbf{k}}^2} \ll \Lambda$  and tends to one for  $\sqrt{k_0^2 + \xi_{\mathbf{k}}^2} \gg \Lambda$ . In this way the infrared singularity of the propagator at  $k_0 = 0$  and  $\xi_{\mathbf{k}} = 0$  (corresponding to the non-interacting Fermi surface in  $\mathbf{k}$ -space) is cut off at scale  $\Lambda$ . A simple choice for  $\Theta_>^\Lambda(K)$ , which we will later adopt in our numerical calculations, is

$$\Theta_>^\Lambda(K) = \Theta(|\xi_{\mathbf{k}}| - \Lambda) \quad (10)$$

where  $\Theta$  is the usual step function. With this choice single-particle states close to the Fermi surface are strictly excluded from the theory. Alternatively, one may also use a smooth cutoff function.

The generating functional for connected Green functions and the effective interaction constructed with  $C^\Lambda$  (instead of  $C$ ) will be denoted by  $\mathcal{G}^\Lambda[\eta, \bar{\eta}]$  and  $\mathcal{V}^\Lambda[\chi, \bar{\chi}]$ , respectively. The original functionals  $\mathcal{G}$  and  $\mathcal{V}$  are recovered in the limit  $\Lambda \rightarrow 0$ . It is not hard to show that the effective interaction satisfies the following exact *renormalization group equation* [20,25]

$$\frac{\partial}{\partial \Lambda} \mathcal{V}^\Lambda[\chi, \bar{\chi}] = \sum_K \dot{C}^\Lambda(K) \frac{\partial^2 \mathcal{V}^\Lambda[\chi, \bar{\chi}]}{\partial \chi_K \partial \bar{\chi}_K} - \sum_K \dot{C}^\Lambda(K) \frac{\partial \mathcal{V}^\Lambda[\chi, \bar{\chi}]}{\partial \chi_K} \frac{\partial \mathcal{V}^\Lambda[\chi, \bar{\chi}]}{\partial \bar{\chi}_K} \quad (11)$$

cutoff introduced above,  $\Lambda_0$  is the maximal value of  $|\xi_{\mathbf{k}}|$ .

An expansion of the functional  $\mathcal{V}^\Lambda[\chi, \bar{\chi}]$  in the renormalization group equation (11) in powers of  $\chi_K$  and  $\bar{\chi}_K$  would lead to Polchinski's [19] flow equations for amputated connected Green functions, which have been applied to the 2D Hubbard model by Zanchi and Schulz [18].

Alternatively, one can also expand with respect to *Wick-ordered* monomials

$$\mathcal{V}^\Lambda[\chi, \bar{\chi}] = \sum_{m=0}^{\infty} \frac{1}{(m!)^2} \sum_{K_1, \dots, K_m} \sum_{K'_1, \dots, K'_m} \times \\ \times V_m^\Lambda(K'_1, \dots, K'_m; K_1, \dots, K_m) e^{-\Delta_{D^\Lambda}} \prod_{j=1}^m \bar{\chi}_{K'_j} \chi_{K_j} \quad (13)$$

The exponent in the Wick-ordering operator is the differential operator

$$\Delta_{D^\Lambda} = \sum_K D^\Lambda(K) \frac{\partial^2}{\partial \chi_K \partial \bar{\chi}_K} \quad (14)$$

with the propagator

$$D^\Lambda(K) = C(K) - C^\Lambda(K) = \frac{\Theta_<^\Lambda(K)}{ik_0 - \xi_K} \quad (15)$$

where  $\Theta_<^\Lambda(K) = 1 - \Theta_>^\Lambda(K)$ . Note that  $D^\Lambda$  contributes in the infrared regime excluded from  $C^\Lambda$ . The Wick-ordered monomials reduce to pure monomials in the limit  $\Lambda \rightarrow 0$ , since  $D^\Lambda(K) \rightarrow 0$  in that limit. Hence, the functions  $V_m^\Lambda$  tend to the usual amputated connected Green functions for  $\Lambda \rightarrow 0$ .

Inserting the expansion (13) for  $\mathcal{V}^\Lambda[\chi, \bar{\chi}]$  on the left hand side of the RG equation (11) yields two terms, with the  $\Lambda$ -derivation acting on the coefficients  $V_m^\Lambda$  or on the Wick-ordered monomials, respectively. Since

$$\frac{\partial}{\partial \Lambda} e^{-\Delta_{D^\Lambda}} \prod_{j=1}^m \bar{\chi}_{K'_j} \chi_{K_j} = \\ - \sum_K \dot{D}^\Lambda(K) \frac{\partial^2}{\partial \chi_K \partial \bar{\chi}_K} e^{-\Delta_{D^\Lambda}} \prod_{j=1}^m \bar{\chi}_{K'_j} \chi_{K_j} \quad (16)$$

and  $\dot{D}^\Lambda = -\dot{C}^\Lambda$ , the second term on the left hand side cancels the first term on the right hand side of (11). Only the second term, quadratic in  $\mathcal{V}^\Lambda$ , remains. Expanding this term with respect to Wick monomials and comparing coefficients, one can express the  $\Lambda$ -derivative of  $V_m^\Lambda$  as a *bilinear* form of all the other functions  $V_n^\Lambda$  [20]. A graphical representation of these flow equations is shown in Fig. 1.

The precise general equation for  $V_m^\Lambda$  has rather complicated combinatorial factors and will not be written here, since we will compute only  $V_2^\Lambda$  in a 1-loop approximation. Note that one internal line in Fig. 1 corresponds to  $\dot{D}^\Lambda$  and the others to the *low* energy propagator  $D^\Lambda$ . Note also that the flow equations are *local* in  $\Lambda$ .

### C. 1-loop equations

To detect dominant instabilities of the system in the weak coupling limit, it is sufficient to truncate the infinite

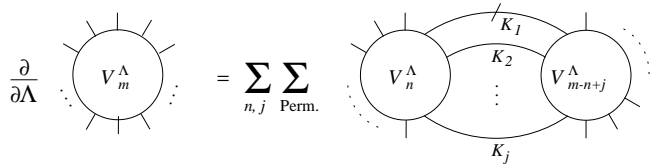


FIG. 1. Diagrammatic representation of the flow equation for the Wick-ordered amputated Green-functions  $V_m^\Lambda$ . The internal line with a slash corresponds to  $\dot{D}^\Lambda$ , the others to  $D^\Lambda$ ; all possible pairings leaving  $m$  ingoing and  $m$  outgoing external legs have to be summed.

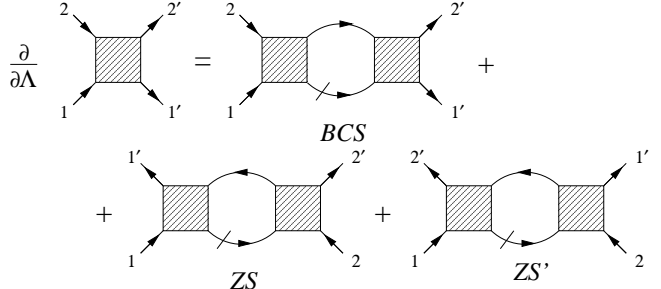


FIG. 2. Flow equation for the vertex function  $\Gamma^\Lambda$  in 1-loop approximation with the particle-particle channel (BCS) and the two particle-hole channels (ZS and ZS').

hierarchy of flow equations described by Fig. 1 at *one-loop* level, and neglect all components of the effective interaction except the two-particle interaction  $V_2^\Lambda$ . Since self-energy corrections are also neglected,  $V_2^\Lambda$  reduces to the one-particle irreducible two-particle *vertex function*, and will therefore be denoted by  $\Gamma^\Lambda$  from now on. Summing all possible pairings of two vertices in a one-loop diagram as in Fig. 2, one obtains the *flow equation*

$$\frac{\partial}{\partial \Lambda} \Gamma^\Lambda(K'_1, K'_2; K_1, K_2) = \\ \frac{1}{\beta V} \sum_{K, K'} \frac{\partial}{\partial \Lambda} [D^\Lambda(K) D^\Lambda(K')] \\ \times \left[ \frac{1}{2} \Gamma^\Lambda(K'_1, K'_2; K, K') \Gamma^\Lambda(K, K'; K_1, K_2) \right. \\ \left. - \Gamma^\Lambda(K'_1, K; K_1, K') \Gamma^\Lambda(K', K'_2; K, K_2) \right. \\ \left. + \Gamma^\Lambda(K'_2, K; K_1, K') \Gamma^\Lambda(K', K'_1; K, K_2) \right] \quad (17)$$

where  $\beta$  is the inverse temperature and  $V$  is the volume of the system. The three terms on the right hand side are the contributions from the Cooper (or BCS) channel and the two zero-sound channels (ZS and ZS'). Note that for translation invariant systems momentum conservation implies that  $\Gamma^\Lambda(K'_1, K'_2; K_1, K_2) \neq 0$  only if  $k_1 + k_2 = k'_1 + k'_2$ , so that the sum over  $k$  and  $k'$  in (17) is reduced to a single energy-momentum sum.

For a spin-rotation invariant system the *spin structure* of the vertex function can be written as

$$\begin{aligned}\Gamma^\Lambda(K'_1, K'_2; K_1, K_2) &= \Gamma_s^\Lambda(k'_1, k'_2; k_1, k_2) S_{\sigma'_1, \sigma'_2; \sigma_1, \sigma_2} + \\ &+ \Gamma_t^\Lambda(k'_1, k'_2; k_1, k_2) T_{\sigma'_1, \sigma'_2; \sigma_1, \sigma_2}\end{aligned}\quad (18)$$

where

$$\begin{aligned}S_{\sigma'_1, \sigma'_2; \sigma_1, \sigma_2} &= \frac{1}{2} (\delta_{\sigma_1 \sigma'_1} \delta_{\sigma_2 \sigma'_2} - \delta_{\sigma_1 \sigma'_2} \delta_{\sigma_2 \sigma'_1}) \\ T_{\sigma'_1, \sigma'_2; \sigma_1, \sigma_2} &= \frac{1}{2} (\delta_{\sigma_1 \sigma'_1} \delta_{\sigma_2 \sigma'_2} + \delta_{\sigma_1 \sigma'_2} \delta_{\sigma_2 \sigma'_1})\end{aligned}\quad (19)$$

are the projection operators on singlet and triplet states in a two-particle spin space, respectively. The antisymmetry of  $\Gamma^\Lambda$  with respect to  $K_1 \leftrightarrow K_2$  or  $K'_1 \leftrightarrow K'_2$  implies that  $\Gamma_s^\Lambda$  is symmetric and  $\Gamma_t^\Lambda$  antisymmetric under exchange of the variables  $k_1$  and  $k_2$  or  $k'_1$  and  $k'_2$ . Carrying out the spin sum in the flow equation one obtains

$$\begin{aligned}\partial_\Lambda \Gamma_\alpha^\Lambda(k'_1, k'_2; k_1, k_2) &= \\ \sum_{i=s,t} \sum_{j=s,t} &[ C_{\alpha ij}^{\text{BCS}} \beta_{ij}^{\text{BCS}}(k'_1, k'_2; k_1, k_2) + \\ &+ C_{\alpha ij}^{\text{ZS}} \beta_{ij}^{\text{ZS}}(k'_1, k'_2; k_1, k_2) + C_{\alpha ij}^{\text{ZS}'} \beta_{ij}^{\text{ZS}'}(k'_1, k'_2; k_1, k_2)]\end{aligned}\quad (20)$$

for  $\alpha = s, t$ , where the coefficients  $C_{\alpha ij}$  can be grouped in matrices

$$\begin{aligned}C_s^{\text{BCS}} &= \begin{pmatrix} 1 & 0 \\ 0 & 0 \end{pmatrix} & C_s^{\text{ZS}} &= -C_s^{\text{ZS}'} = \frac{1}{4} \begin{pmatrix} -1 & 3 \\ 3 & 3 \end{pmatrix} \\ C_t^{\text{BCS}} &= \begin{pmatrix} 0 & 0 \\ 0 & 1 \end{pmatrix} & C_t^{\text{ZS}} &= C_t^{\text{ZS}'} = \frac{1}{4} \begin{pmatrix} 1 & 1 \\ 1 & 5 \end{pmatrix}\end{aligned}\quad (21)$$

and the “ $\beta$ -functions” are given by

$$\begin{aligned}\beta_{ij}^{\text{BCS}}(k'_1, k'_2; k_1, k_2) &= \frac{1}{2\beta V} \sum_{k, k'} \partial_\Lambda [D^\Lambda(k) D^\Lambda(k')] \times \\ &\times \Gamma_i^\Lambda(k'_1, k'_2; k, k') \Gamma_j^\Lambda(k, k'; k_1, k_2) \\ \beta_{ij}^{\text{ZS}}(k'_1, k'_2; k_1, k_2) &= -\frac{1}{\beta V} \sum_{k, k'} \partial_\Lambda [D^\Lambda(k) D^\Lambda(k')] \times \\ &\times \Gamma_i^\Lambda(k'_1, k; k_1, k') \Gamma_j^\Lambda(k', k'_2; k, k_2) \\ \beta_{ij}^{\text{ZS}'}(k'_1, k'_2; k_1, k_2) &= -\beta_{ij}^{\text{ZS}}(k'_2, k'_1; k_1, k_2)\end{aligned}\quad (22)$$

We finally list some useful relations for the vertex function following from general *symmetries*. Time-reversal invariance implies

$$\begin{aligned}\Gamma^\Lambda(K'_1, K'_2; K_1, K_2) &= \sigma'_1 \sigma'_2 \sigma_1 \sigma_2 \times \\ &\times \Gamma^\Lambda(\mathcal{R}K_1, \mathcal{R}K_2; \mathcal{R}K'_1, \mathcal{R}K'_2)\end{aligned}\quad (23)$$

where  $\mathcal{R}K = (k_0, -\mathbf{k}, -\sigma)$  for  $K = (k_0, \mathbf{k}, \sigma)$ , and the number 1 (-1) is assigned to  $\sigma = \uparrow$  ( $\downarrow$ ) in the prefactor. Assuming in addition spatial reflection invariance and spin rotation invariance, one obtains

$$\Gamma^\Lambda(K'_1, K'_2; K_1, K_2) = \Gamma^\Lambda(K_1, K_2; K'_1, K'_2)\quad (24)$$

From the behavior under complex conjugation

$$\bar{\Gamma}^\Lambda(K'_1, K'_2; K_1, K_2) = \Gamma^\Lambda(\bar{K}_1, \bar{K}_2; \bar{K}'_1, \bar{K}'_2)\quad (25)$$

with  $\bar{K} = (-k_0, \mathbf{k}, \sigma)$  one can then deduce that the vertex function  $\Gamma^\Lambda(K'_1, K'_2; K_1, K_2)$  is real, if all the energy variables vanish.

## D. Susceptibilities

To identify possible instabilities of the system we compute various susceptibilities, i.e. the linear response of the system to small external fields.

Application of an external field  $h$  leads to an additional contribution to the action

$$V'[h; \psi, \bar{\psi}] = - \sum_q [\bar{h}(q) O(q) + h(q) \bar{O}(q)]\quad (26)$$

where  $O(q)$  is a bilinear form in the Grassmann variables,  $\bar{O}(q)$  its hermitian conjugate, and  $\bar{h}(q)$  is the complex conjugate of  $h(q)$ . We will compute the response to fields coupling to the *charge density*

$$\rho(q) = \sum_{k, \sigma} \bar{\psi}_{k-q, \sigma} \psi_{k, \sigma}\quad (27)$$

and the *spin density* in  $z$ -direction

$$s^z(q) = \sum_k [\bar{\psi}_{k-q, \uparrow} \psi_{k, \uparrow} - \bar{\psi}_{k-q, \downarrow} \psi_{k, \downarrow}]\quad (28)$$

and also the response to pairing fields coupling to the *singlet pair* operator

$$\Delta(q) = \sum_{k, \sigma} d(\mathbf{k} + \mathbf{q}/2) \psi_{k+q, \uparrow} \psi_{-k, \downarrow}\quad (29)$$

where  $d(\mathbf{k})$  is a function with even parity specifying the orbital symmetry of the pairing operator ( $s$ -wave,  $d$ -wave etc.). The linear response of the expectation value

$$m(q) = V^{-1} \langle O(q) \rangle = \frac{1}{V} \frac{\partial \log \mathcal{Z}[h]}{\partial \bar{h}(q)}\quad (30)$$

with the partition function

$$\mathcal{Z}[h] = \int d\mu_C[\psi, \bar{\psi}] e^{-V[\psi, \bar{\psi}] - V'[h; \psi, \bar{\psi}]}\quad (31)$$

is given by the susceptibility

$$\chi(q) = \left. \frac{\partial m(q)}{\partial \bar{h}(q)} \right|_{h=0} = V^{-1} \langle O(q) \bar{O}(q) \rangle|_{h=0}\quad (32)$$

We consider only systems which are translation invariant, spin-rotation invariant, and charge conserving in

the absence of the external field  $h$ . In the normal (not symmetry-broken) phase the expectation values  $\langle O(q) \rangle$  then vanish for  $h(q) \rightarrow 0$ , except the expectation value  $\langle \rho(0) \rangle$ , which yields the average particle number of the system.

The renormalization group equation (11) is not affected by the presence of the additional term  $V'$  in the bare action, since an arbitrary many-body interaction was allowed anyway. Only the initial condition of the

$$\mathcal{V}^\Lambda[h; \chi, \bar{\chi}] = \sum_{m,n=0}^{\infty} \frac{1}{m!n!} \sum_{K'_1, \dots, K'_m} \sum_{K_1, \dots, K_n} V_{mn}^\Lambda([h]; K'_1, \dots, K'_m; K_1, \dots, K_n) e^{-\Delta_{D^\Lambda}} \bar{\chi}_{K'_1} \dots \bar{\chi}_{K'_m} \chi_{K_n} \dots \chi_{K_1} \quad (34)$$

To obtain the *linear* response of the system, we expand the effective  $m$ -body interactions  $V_m^\Lambda$  (or its generalization  $V_{mn}^\Lambda$ ) in powers of  $h$ . The effective 0-body interaction can be expanded as

$$V_0^\Lambda[h] = V_0^\Lambda - V \sum_q \chi^\Lambda(q) \bar{h}(q) h(q) + \mathcal{O}(h^3) \quad (35)$$

Note that  $V_0^\Lambda[h]$  converges to the grand-canonical potential  $\Omega[h] = -\log \mathcal{Z}[h]$  for  $\Lambda \rightarrow 0$ , and  $\chi^\Lambda(q)$  converges to the susceptibility  $\chi(q)$ . If  $h$  couples to the charge density, there is also a linear contribution  $-N^\Lambda[h(0) + \bar{h}(0)]$  in the expansion of  $V_0^\Lambda[h]$ , where  $N^\Lambda$  converges to the average particle number for  $\Lambda \rightarrow 0$ . For a field coupling to charge or spin density, the effective 1-body interaction becomes

$$\begin{aligned} V_1^\Lambda([h]; K'; K) &= V_1^\Lambda(K'; K) - \\ &- \sum_q [R^\Lambda(q; K'; K) \bar{h}(q) + \text{h.c.}] + \mathcal{O}(h^2) \end{aligned} \quad (36)$$

The spin structure of the renormalized vertex  $R^\Lambda$  is

$$R^\Lambda(q; K'; K) = \delta_{\sigma'\sigma} R_C^\Lambda(q; k'; k) \quad (37)$$

for the charge vertex and

$$R^\Lambda(q; K'; K) = \sigma \delta_{\sigma'\sigma} R_S^\Lambda(q; k'; k) \quad (38)$$

for the spin vertex. For a pairing field,  $V_1^\Lambda$  has only quadratic terms in  $h$ , but the off-diagonal effective interactions

$$\begin{aligned} V_{0,2}^\Lambda([h]; K_1, K_2) &= -2 \sum_q R^\Lambda(q; K_1, K_2) \bar{h}(q) + \mathcal{O}(h^2) \\ V_{2,0}^\Lambda([h]; K'_1, K'_2) &= -2 \sum_q \bar{R}^\Lambda(q; K'_1, K'_2) h(q) + \mathcal{O}(h^2) \end{aligned} \quad (39)$$

have linear (and higher order) contributions. The spin structure of the renormalized singlet pairing vertex is

$$R^\Lambda(q; K_1, K_2) = \sigma_1 \delta_{\sigma_1, -\sigma_2} R_s^\Lambda(q; k_1, k_2) \quad (40)$$

flow is modified to

$$\mathcal{V}^{\Lambda_0}[h; \chi, \bar{\chi}] = V[\chi, \bar{\chi}] + V'[h; \chi, \bar{\chi}] \quad (33)$$

which leads to an  $h$ -dependent effective interaction  $\mathcal{V}^\Lambda[h; \chi, \bar{\chi}]$ . When a pairing field is coupled to the system, the expansion of  $\mathcal{V}^\Lambda[h; \chi, \bar{\chi}]$  with respect to Wick-ordered monomials will also contain monomials where the number of creation and annihilation variables is not equal, and Eq. (13) must be generalized to

Effective two- and many-body interactions can be expanded similarly. Inserting the expansions of the effective interactions  $V_{mn}^\Lambda$  into the flow equations and comparing the coefficients of contributions with equal powers in the external field, one obtains flow equations for these coefficients, especially for  $\chi^\Lambda$  and  $R^\Lambda$ .

We will again truncate the infinite hierarchy of flow equations at 1-loop level, and neglect (zero-field) self-energy terms by setting  $V_1^\Lambda(K'; K) = 0$ . To obtain the linear response susceptibility it is then sufficient to solve the two flow equations for the susceptibility  $\chi^\Lambda$  and the renormalized charge, spin, or pairing vertex  $R^\Lambda$  represented diagrammatically in Fig. 3. If  $h$  couples to the charge or spin density, these equations read

$$\begin{aligned} \frac{\partial}{\partial \Lambda} \chi^\Lambda(q) &= \frac{1}{\beta V} \sum_{K, K'} \partial_\Lambda [D^\Lambda(K) D^\Lambda(K')] \times \\ &\times R^\Lambda(q; K'; K) R^\Lambda(-q; K; K') \end{aligned} \quad (41)$$

and

$$\begin{aligned} \frac{\partial}{\partial \Lambda} R^\Lambda(q; K'_1; K_1) &= -\frac{1}{\beta V} \sum_{K, K'} \partial_\Lambda [D^\Lambda(K) D^\Lambda(K')] \times \\ &\times R^\Lambda(q; K'; K) \Gamma^\Lambda(K'_1, K; K_1, K') \end{aligned} \quad (42)$$

with the initial condition  $R^{\Lambda_0}(q; K'; K) = \delta_{\sigma'\sigma} \delta_{k-k', q}$  for the charge and  $R^{\Lambda_0}(q; K'; K) = \sigma \delta_{\sigma'\sigma} \delta_{k-k', q}$  for the spin vertex part. Note that  $R^\Lambda(q; K'; K) \neq 0$  only if  $k' = k - q$ . If  $h$  couples to pair creation and annihilation operators, the flow equations become

$$\begin{aligned} \frac{\partial}{\partial \Lambda} \chi^\Lambda(q) &= -\frac{2}{\beta V} \sum_{K_1, K_2} \partial_\Lambda [D^\Lambda(K_1) D^\Lambda(K_2)] \times \\ &\times R^\Lambda(q; K_1, K_2) \bar{R}^\Lambda(q; K_1, K_2) \end{aligned} \quad (43)$$

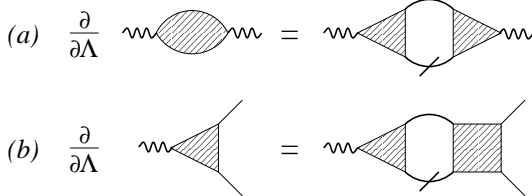


FIG. 3. Flow equations for (a) the susceptibilities  $\chi^\Lambda$  and (b) the response vertices  $R^\Lambda$  in 1-loop approximation.

and

$$\begin{aligned} \frac{\partial}{\partial \Lambda} R^\Lambda(q; K_1, K_2) = & \frac{1}{2\beta V} \sum_{K'_1, K'_2} \partial_\Lambda [D^\Lambda(K'_1) D^\Lambda(K'_2)] \times \\ & \times R^\Lambda(q; K'_1, K'_2) \Gamma^\Lambda(K'_1, K'_2; K_1, K_2) \end{aligned} \quad (44)$$

with the initial condition  $R^{\Lambda_0}(q; K_1, K_2) = \sigma_1 \delta_{\sigma_1, -\sigma_2} \delta_{k_1 + k_2, q} d\left(\frac{\mathbf{k}_1 - \mathbf{k}_2}{2}\right)$ . Note that  $R^\Lambda(q; K_1, K_2) \neq 0$  only if  $k_1 + k_2 = q$ . The initial condition for the susceptibility is  $\chi^{\Lambda_0}(q) = 0$  in all cases.

The vertex function  $\Gamma^\Lambda$  is obtained by solving the flow equations (17) in the absence of a perturbing field. One can then solve the linear differential equation for  $R^\Lambda$  and finally integrate the flow equation for  $\chi^\Lambda$ . Note that for the special case of a flat fermi surface these 1-loop equations have the same structure as the so-called fast parquet equations [17], but here the flow variable is the cutoff  $\Lambda$  instead of an external energy or momentum variable.

### III. APPLICATION TO THE 2D HUBBARD MODEL

We will now apply the general renormalization group method derived in the previous section to the two-dimensional Hubbard model, the main aim being an analysis of the leading instabilities of the system at weak coupling.

#### A. Hubbard model and Fermi surface

The Hubbard model [2] is a lattice electron model with the simple Hamiltonian

$$H = \sum_{\mathbf{i}, \mathbf{j}} \sum_{\sigma} t_{\mathbf{i}\mathbf{j}} c_{\mathbf{i}\sigma}^\dagger c_{\mathbf{j}\sigma} + U \sum_{\mathbf{j}} n_{\mathbf{j}\uparrow} n_{\mathbf{j}\downarrow}, \quad (45)$$

where  $c_{\mathbf{i}\sigma}^\dagger$  and  $c_{\mathbf{i}\sigma}$  are the usual creation and annihilation operators for fermions with spin projection  $\sigma \in \{\uparrow, \downarrow\}$  on a lattice site  $\mathbf{i}$ . We consider the Hubbard model with a repulsive interaction  $U > 0$  on a (two-dimensional) square lattice with a hopping amplitude

$$t_{\mathbf{i}\mathbf{j}} = \begin{cases} -t & \text{if } \mathbf{i} \text{ and } \mathbf{j} \text{ are nearest neighbors} \\ -t' & \text{if } \mathbf{i} \text{ and } \mathbf{j} \text{ are next-nearest neighbors} \\ 0 & \text{else} \end{cases} \quad (46)$$

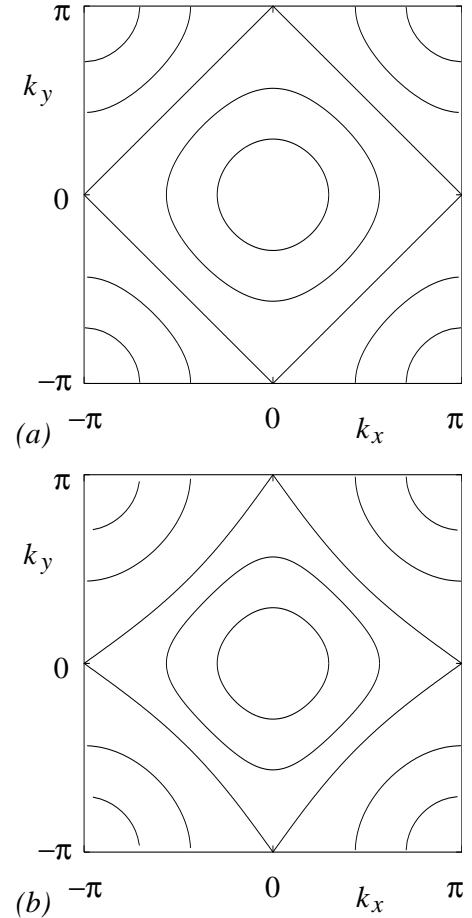


FIG. 4. The Fermi surfaces of the non-interacting 2D Hubbard model with  $t' = 0$  (a) and  $t' = -0.16t$  (b) for various choices of the chemical potential  $\mu$ .

The corresponding dispersion relation of non-interacting particles is

$$\epsilon_{\mathbf{k}} = -2t(\cos k_x + \cos k_y) - 4t'(\cos k_x \cos k_y) \quad (47)$$

This dispersion relation has saddle points at  $\mathbf{k} = (0, \pi)$  and  $(\pi, 0)$ , which lead to logarithmic van Hove singularities in the non-interacting density of states at the energy  $\epsilon = \epsilon_{vH} = 4t'$ . In Fig. 4 we show the Fermi surfaces of the non-interacting system for various electron densities  $n$  for the case without next-nearest neighbor hopping ( $t' = 0$ ) and a case with  $t' < 0$ .

For a chemical potential  $\mu = \epsilon_{vH}$  the Fermi surface contains the van Hove points. In this case a perturbative calculation of the two-particle vertex function leads to several infrared divergencies already at second order in  $U$ , i.e. at 1-loop level (see the Feynman diagrams in Fig. 2) [8–10]. In particular, the particle-particle channel diverges as  $\log^2$  for vanishing total momentum  $\mathbf{k}_1 + \mathbf{k}_2$ ,

and logarithmically for  $\mathbf{k}_1 + \mathbf{k}_2 = (\pi, \pi)$ . The particle-hole channel diverges logarithmically for vanishing momentum transfer; for momentum transfer  $(\pi, \pi)$  it diverges logarithmically if  $t' \neq 0$  and as  $\log^2$  in the special case  $t' = 0$ . Note that  $\mu = 0$  for  $t' = 0$  corresponds to half-filling ( $n = 1$ ). For  $t' = 0$  there are also logarithmic divergences for all momentum transfers parallel to  $(\pi, \pi)$  or  $(\pi, -\pi)$  due to the strong nesting of the square shaped Fermi surface. For  $\mu \neq \epsilon_{\text{vH}}$  only the usual logarithmic Cooper singularity at zero total momentum in the particle-particle channel remains. However, the additional singularities at  $\mu = \epsilon_{\text{vH}}$  lead clearly to largely enhanced contributions for small  $\mu - \epsilon_{\text{vH}}$ , especially if  $t'$  is also small.

Hence, for small  $\mu - \epsilon_{\text{vH}}$  one has to deal with competing divergencies in different channels. This problem can be treated systematically by the RG method described in Sec. II.

---


$$\partial_\Lambda \Gamma_\alpha^\Lambda(\mathbf{k}'_1, \mathbf{k}'_2; \mathbf{k}_1, \mathbf{k}_2) = \sum_{i=s,t} \sum_{j=s,t} \left[ C_{\alpha ij}^{\text{BCS}} \beta_{ij}^{\text{BCS}}(\mathbf{k}'_1, \mathbf{k}'_2; \mathbf{k}_1, \mathbf{k}_2) + C_{\alpha ij}^{\text{ZS}} \beta_{ij}^{\text{ZS}}(\mathbf{k}'_1, \mathbf{k}'_2; \mathbf{k}_1, \mathbf{k}_2) + C_{\alpha ij}^{\text{ZS}'} \beta_{ij}^{\text{ZS}'}(\mathbf{k}'_1, \mathbf{k}'_2; \mathbf{k}_1, \mathbf{k}_2) \right] \quad (49)$$

for  $\alpha = s, t$ , where the  $\beta$ -functions are now frequency independent and read

$$\begin{aligned} \beta_{ij}^{\text{BCS}}(\mathbf{k}'_1, \mathbf{k}'_2; \mathbf{k}_1, \mathbf{k}_2) &= \frac{1}{2V} \sum_{\mathbf{k}, \mathbf{k}'} \partial_\Lambda [\Theta_<^\Lambda(\mathbf{k}) \Theta_<^\Lambda(\mathbf{k}')] \frac{f(-\xi_{\mathbf{k}}) - f(\xi_{\mathbf{k}'})}{\xi_{\mathbf{k}} + \xi_{\mathbf{k}'}} \Gamma_i^\Lambda(\mathbf{k}'_1, \mathbf{k}'_2; \mathbf{k}, \mathbf{k}') \Gamma_j^\Lambda(\mathbf{k}, \mathbf{k}'; \mathbf{k}_1, \mathbf{k}_2) \\ \beta_{ij}^{\text{ZS}}(\mathbf{k}'_1, \mathbf{k}'_2; \mathbf{k}_1, \mathbf{k}_2) &= -\frac{1}{V} \sum_{\mathbf{k}, \mathbf{k}'} \partial_\Lambda [\Theta_<^\Lambda(\mathbf{k}) \Theta_<^\Lambda(\mathbf{k}')] \frac{f(\xi_{\mathbf{k}}) - f(\xi_{\mathbf{k}'})}{\xi_{\mathbf{k}} - \xi_{\mathbf{k}'}} \Gamma_i^\Lambda(\mathbf{k}'_1, \mathbf{k}; \mathbf{k}_1, \mathbf{k}') \Gamma_j^\Lambda(\mathbf{k}', \mathbf{k}_2; \mathbf{k}, \mathbf{k}_2) \\ \beta_{ij}^{\text{ZS}'}(\mathbf{k}'_1, \mathbf{k}'_2; \mathbf{k}_1, \mathbf{k}_2) &= -\beta_{ij}^{\text{ZS}}(\mathbf{k}'_2, \mathbf{k}'_1; \mathbf{k}_1, \mathbf{k}_2) \end{aligned} \quad (50)$$

with the Fermi function  $f(\xi) = [e^{\beta\xi} + 1]^{-1}$ . Note that momentum conservation implies that  $\mathbf{k}$  and  $\mathbf{k}'$  are related by  $\mathbf{k} + \mathbf{k}' = \mathbf{k}_1 + \mathbf{k}_2$  in the Cooper channel and by  $\mathbf{k} + \mathbf{k}' = \mathbf{k}' + \mathbf{k}_1$  in the zero sound channel, such that only one independent momentum variable has to be summed.

For a step cutoff function  $\Theta_<^\Lambda(\mathbf{k}) = \Theta(\Lambda - |\xi_{\mathbf{k}}|)$  one has

$$\partial_\Lambda [\Theta_<^\Lambda(\mathbf{k}) \Theta_<^\Lambda(\mathbf{k}')] = \delta(\Lambda - |\xi_{\mathbf{k}}|) \Theta(\Lambda - |\xi_{\mathbf{k}'}|) + \mathbf{k} \leftrightarrow \mathbf{k}' \quad (51)$$

such that the  $\mathbf{k}$ -sum can be reduced to a one-dimensional integral in the thermodynamic limit. To this end we substitute  $k_x$  and  $k_y$  by the new variables  $\xi = \xi_{\mathbf{k}}$  and the angle  $\phi$  between  $\mathbf{k}$  and the  $x$ -axis in  $\mathbf{k}$ -space, and use

$$\begin{aligned} \frac{1}{V} \sum_{\mathbf{k}} \dots &\rightarrow \\ \int \frac{dk_x}{2\pi} \frac{dk_y}{2\pi} \dots &= \frac{1}{(2\pi)^2} \int d\xi \int_0^{2\pi} d\phi J(\xi, \phi) \dots \end{aligned} \quad (52)$$

## B. Parameterization of the vertex function

We now prepare for a computation of the 1-loop flow of the vertex function and susceptibilities. The flow equations derived in Sec. II cannot be solved analytically. Even a numerical solution is not possible with the full energy and momentum dependence of the vertex function, which must therefore be suitably simplified.

The dependence of the vertex function on energy variables can be neglected completely without much damage, because it is absent in the bare interaction, and irrelevant (in the sense of power counting) in the low-energy limit (see, for example, Ref. [26]). We therefore approximate

$$\Gamma_\alpha^\Lambda(k'_1, k'_2; k_1, k_2) \approx \Gamma_\alpha^\Lambda(\mathbf{k}'_1, \mathbf{k}'_2; \mathbf{k}_1, \mathbf{k}_2) \quad (48)$$

Choosing an energy independent cutoff function  $\Theta_<^\Lambda(\mathbf{k})$ , the Matsubara sums on the right hand side of the flow equations can then be performed analytically. One thus obtains

---

where  $J(\xi, \phi)$  is the Jacobian associated with the transformation of variables. Since the integrand contains a factor  $\delta(\Lambda - |\xi|)$ , the  $\xi$ -integration can be performed by hand, leaving only the angular integral over  $\phi$  to be done numerically.

The flow equation can be solved only if also the momentum dependence of the vertex function is simplified. At least for weak coupling (in practice also for moderate ones), the vertex function acquires strong momentum dependences only for momenta close to the Fermi surface. Note that for the Hubbard model the bare vertex function  $\Gamma^{\Lambda_0}$  does not depend on momentum at all. Instabilities are signalled by divergencies of the vertex function  $\Gamma^\Lambda$  for momenta close to the Fermi surface and small  $\Lambda$ . Hence we will focus on the flow of the vertex function with momenta close to the Fermi surface.

The intermediate momenta  $\mathbf{k}$  and  $\mathbf{k}'$  are constrained to a momentum shell around the Fermi surface, since  $|\xi_{\mathbf{k}}|, |\xi_{\mathbf{k}'}| \leq \Lambda$  (see Eq. (51)). Hence, the values of the vertex function at momenta within that  $\Lambda$ -shell govern

their own flow.

For fixed finite  $\Lambda$ , the dependence of  $\Gamma_\alpha^\Lambda(\mathbf{k}'_1, \mathbf{k}'_2; \mathbf{k}_1, \mathbf{k}_2)$  on  $\xi_{\mathbf{k}_1}$  etc. is regularized by the cutoff for  $|\xi_{\mathbf{k}_1}|, \dots < \Lambda$ . For momenta within the  $\Lambda$ -shell one may therefore approximate the vertex function by

$$\Gamma_\alpha^\Lambda(\mathbf{k}'_1, \mathbf{k}'_2; \mathbf{k}_1, \mathbf{k}_2) \approx \Gamma_\alpha^\Lambda(\mathbf{k}'_{F1}, \mathbf{k}_{F1} + \mathbf{k}_{F2} - \mathbf{k}'_{F1}; \mathbf{k}_{F1}, \mathbf{k}_{F2}) \quad (53)$$

where  $\mathbf{k}_{F1}$  etc. are projections of  $\mathbf{k}_1$  etc. on the Fermi surface (see Fig. 5). Note that strong momentum dependences of the effective vertex are built up only by contributions with intermediate momenta  $\mathbf{k}$  and  $\mathbf{k}'$  (on the right hand side of the flow equations) which are close to the Fermi surface, because for such momenta the fractions  $\frac{f(\mp\xi_{\mathbf{k}}) - f(\xi_{\mathbf{k}'})}{\xi_{\mathbf{k}} \pm \xi_{\mathbf{k}'}}$  can be big. Hence, for the most important momenta, the error made by the projection is relatively small (even if  $\Lambda$  is not small), because these momenta are close to their projected counterparts. The projected vertex function can be parameterized by three angles  $\phi_1, \phi_2, \phi_3$  associated with  $\mathbf{k}_{F1}$ ,  $\mathbf{k}_{F2}$  and  $\mathbf{k}'_{F1}$ , respectively, i.e.

$$\Gamma_\alpha^\Lambda(\mathbf{k}'_{F1}, \mathbf{k}_{F1} + \mathbf{k}_{F2} - \mathbf{k}'_{F1}; \mathbf{k}_{F1}, \mathbf{k}_{F2}) = \Gamma_\alpha^\Lambda(\phi_1, \phi_2, \phi_3) \quad (54)$$

The angular dependence turns out to be strong for small  $\Lambda$  and cannot be neglected.

With the above projection procedure only functional dependences which are irrelevant in the low-energy limit have been neglected (see, for example, Ref. [26]). The approximation (53) is asymptotically exact for  $\Lambda \rightarrow 0$  (for momenta within the  $\Lambda$ -shell) and, for the Hubbard model, also for  $\Lambda = \Lambda_0$ . At intermediate stages of the flow there are of course corrections. To assess their importance, we have refined the parameterization of the vertex function in some test runs by using a second surface of constant energy in momentum space as a target for momentum projections. In addition to the Fermi surface a canonical choice is the *van Hove surface* defined by  $\epsilon_{\mathbf{k}} = \epsilon_{vH}$ , where  $\epsilon_{vH}$  is the energy at which the density of states has a van Hove singularity due to saddle points of  $\epsilon_{\mathbf{k}}$ . Momenta are then projected on that surface (Fermi or van Hove) which is energetically closer. In this way scattering processes between van Hove points, which are particularly important at scales  $\Lambda = |\epsilon_{vH} - \mu|$ , are treated more accurately. In addition to the three angles  $\phi_1, \phi_2, \phi_3$  one needs three binary variables  $\nu_1, \nu_2, \nu_3$  to label the closest projection surface for  $\mathbf{k}_1, \mathbf{k}_2$  and  $\mathbf{k}'_1$ .

The parameterization of the vertex parts  $R^\Lambda$  required for the computation of susceptibilities is done in a similar fashion. We concentrate on *static* susceptibilities ( $q_0 = 0$ ) and neglect the (irrelevant) energy dependence of  $R^\Lambda$ . For the charge and spin density vertex we approximate

$$R_{C,S}^\Lambda(\mathbf{q}; \mathbf{k}'; \mathbf{k}) \approx R_{C,S}^\Lambda(\mathbf{q}; \mathbf{k}_F - \mathbf{q}; \mathbf{k}_F) \quad (55)$$

where  $\mathbf{k}_F$  is the projection of  $\mathbf{k}$  on the Fermi surface. The pairing susceptibility is computed only for the most

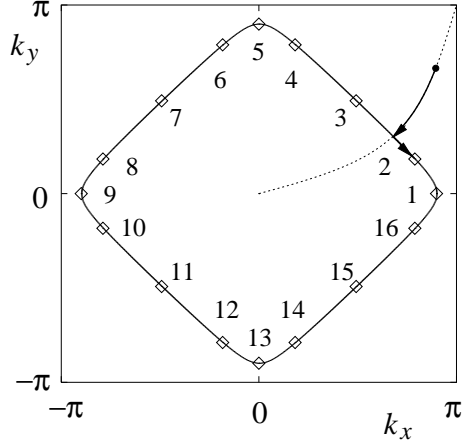


FIG. 5. Projection of momenta on the Fermi surface; discretization and labelling of angle variables.

interesting case of vanishing total momentum  $\mathbf{q} = 0$ . The corresponding vertex part is approximated by

$$R_s^\Lambda(\mathbf{0}; \mathbf{k}, -\mathbf{k}) \approx R_s^\Lambda(\mathbf{0}; \mathbf{k}_F, -\mathbf{k}_F) \quad (56)$$

The projection approximation for the vertex parts is again exact for  $\Lambda = \Lambda_0$  and asymptotically exact for  $\Lambda \rightarrow 0$ . It can also be improved for intermediate  $\Lambda$  by projecting momenta either on the Fermi surface or on the van Hove surface, whichever is closer.

The behavior of the *compressibility*  $\chi_C = \partial n / \partial \mu = \chi_C(\mathbf{0})$  and the *homogeneous spin susceptibility*  $\chi_S = \chi_S(\mathbf{0})$  cannot be obtained directly from the flow equations for  $\chi_{C,S}^\Lambda(\mathbf{q})$ . The problem is that  $\chi_{C,S}^\Lambda(\mathbf{0})$  vanishes for all  $\Lambda > 0$  (at zero temperature), since the infrared cutoff blocks particle-hole excitations with an infinitesimal momentum transfer. We will therefore compute  $\chi_C$  and  $\chi_S$  from the effective quasi-particle interaction

$$f_{\mathbf{k}_F \mathbf{k}'_F}^{\sigma \sigma' \Lambda} = Z_{\mathbf{k}_F}^\Lambda Z_{\mathbf{k}'_F}^\Lambda \Gamma^\Lambda(\mathbf{k}_F \sigma, \mathbf{k}'_F \sigma'; \mathbf{k}_F \sigma, \mathbf{k}'_F \sigma') \quad (57)$$

Note that the forward scattering limit (zero momentum and energy transfer) of the two-particle vertex is unique for  $\Lambda > 0$  and converges to the quasi-particle interaction for  $\Lambda \rightarrow 0$  and  $\mathbf{k}_F \neq \mathbf{k}'_F$  [27]. The wave function renormalization factor  $Z_{\mathbf{k}_F}^\Lambda$  is one in our calculation because we have neglected self-energy contributions. Following the usual Fermi liquid arguments [28] one obtains the compressibility and the homogeneous spin susceptibility as

$$\chi_{C,S} = 2 \int \frac{d^2 k}{(2\pi)^2} X_{\mathbf{k}_F}^{C,S} \delta(\epsilon_{\mathbf{k}} - \mu) \quad (58)$$

where  $X_{\mathbf{k}_F}^{C,S}$  is the solution of the inhomogeneous linear integral equation

$$X_{\mathbf{k}_F}^{C,S} + 2 \int \frac{d^2 k'}{(2\pi)^2} f_{\mathbf{k}_F \mathbf{k}'_F}^{C,S} X_{\mathbf{k}'_F}^{C,S} \delta(\epsilon_{\mathbf{k}'} - \mu) = 1 \quad (59)$$

with  $f_{\mathbf{k}_F \mathbf{k}'_F}^{C,S} = \frac{1}{2} \left( f_{\mathbf{k}_F \mathbf{k}'_F}^{\sigma\sigma} \pm f_{\mathbf{k}_F \mathbf{k}'_F}^{\sigma,-\sigma} \right)$ . In a non-interacting system one would obtain  $X_{\mathbf{k}_F}^{C,S} = 1$ . The quantity

$$\frac{\partial s_{\mathbf{k}_F}}{\partial \mu} = \frac{1}{|\mathbf{v}_{\mathbf{k}_F}|} X_{\mathbf{k}_F}^C \quad (60)$$

with the velocity  $\mathbf{v}_{\mathbf{k}} = \nabla_{\mathbf{k}} \epsilon_{\mathbf{k}}$  describes the linear response of the Fermi surface in  $\mathbf{k}_F$  (a shift along the normal vector) for a small shift of the chemical potential.

For a concrete numerical solution of the flow equations the angular dependence of the vertex function is discretized, with a finer mesh in the vicinity of the saddle points of  $\epsilon_{\mathbf{k}}$  at  $(\pi, 0)$  and  $(0, \pi)$ , as shown in Fig. 5. One is thus left with a finite (though very large) number of flowing coupling constants. If not stated otherwise, we have used 16 points on the Fermi surface to discretize the vertex function, corresponding to 672 independent (i.e. not symmetry-related) coupling constants, if the fermi level lies at the van Hove energy  $\epsilon_{vHS}$ , and 846 couplings otherwise. With the addition of 16 points on the van Hove surface one has to deal with 4728 flowing couplings.

### C. Results

We have computed the flow of the vertex function and the susceptibilities for several choices of the bare interaction  $U > 0$ , the next-nearest neighbor hopping amplitude  $t' \leq 0$  and the chemical potential  $\mu$ , where  $t'$  and  $\mu$  have been chosen such that the Fermi surface is on or close to the van Hove points of  $\epsilon_{\mathbf{k}}$ , and the particle density is close to half-filling.

In all cases the vertex function develops a strong momentum dependence for small  $\Lambda$  with divergencies for several momenta at some critical scale  $\Lambda_c > 0$ , which vanishes exponentially  $U \rightarrow 0$ . To see which physical instability is associated with the diverging vertex function we have computed the following susceptibilities:

- i) commensurate antiferromagnetic spin susceptibility  $\chi_S(\pi, \pi)$ ,
- ii) incommensurate spin susceptibility  $\chi_S(\mathbf{q})$  with  $\mathbf{q} = (\pi - \delta, \pi)$  and  $\mathbf{q} = (1 - \delta)(\pi, \pi)$  [29],
- iii) commensurate charge susceptibility  $\chi_C(\pi, \pi)$ ,
- iv) singlet pair susceptibilities with form factors [3]

$$d(\mathbf{k}) = \begin{cases} 1 & (s\text{-wave}) \\ \frac{1}{\sqrt{2}}(\cos k_x + \cos k_y) & (\text{extended } s\text{-wave}) \\ \frac{1}{\sqrt{2}}(\cos k_x - \cos k_y) & (d\text{-wave } d_{x^2-y^2}) \\ \sin k_x \sin k_y & (d\text{-wave } d_{xy}) \end{cases} \quad (61)$$

Some of these susceptibilities diverge together with the vertex function at the scale  $\Lambda_c$ . Depending on the choice of  $U$ ,  $t'$  and  $\mu$  the strongest divergence is found for the

commensurate or incommensurate spin susceptibility or for the pair susceptibility with  $d_{x^2-y^2}$  symmetry.

We will now present explicit results for the flow of the two-particle vertex and susceptibilities for a coupling strength  $U = t$ , which is much smaller than the bandwidth  $W = 8t$  and therefore safely in the weak coupling regime. All energy scales will be plotted in units of  $t$ . To exhibit the interaction-induced renormalizations of the susceptibilities, we plot the flow of the ratio  $\chi^{\Lambda}/\chi_0^{\Lambda}$ , where  $\chi_0^{\Lambda}$  is the susceptibility of the non-interacting system at scale  $\Lambda$ , as obtained from the flow equations for  $U = 0$ . We show examples for the flow of  $\chi_0^{\Lambda}$  in the Appendix. Note that the non-interacting susceptibilities  $\chi_0^{\Lambda}$  are all finite for  $\Lambda > 0$ , such that a divergence of  $\chi^{\Lambda}$  at a finite scale  $\Lambda_c$  implies a diverging ratio  $\chi^{\Lambda}/\chi_0^{\Lambda}$  and vice versa.

In Fig. 6 we show the flow for  $t' = 0$  and  $\mu = -0.005$ , corresponding to a density  $n = 0.995$ , i.e. almost at half-filling. Here and in the following we plot the singlet part of the vertex function for a selected choice of momenta on the Fermi surface, including those momenta for which the vertex function renormalizes most strongly. The singlet vertex function has its largest values for umklapp scattering along the diagonal of the Brillouin zone, but also forward and Cooper scattering of particles on opposite sides of the almost square Fermi surface are strongly enhanced. Scattering amplitudes for momenta near the van Hove points diverge a bit more slowly. The triplet part of the vertex function is renormalized mostly for forward and Cooper scattering, but generally more weakly than the singlet part. The spin susceptibility with an antiferromagnetic wave vector clearly dominates over pairing susceptibilities in this case. The incommensurate spin susceptibilities are indistinguishable from the commensurate one in Fig. 6 because the incommensurability parameter  $\delta$  is almost zero so close to half-filling (see Ref. [29]). Note also that the susceptibility ratios for isotropic and extended  $s$ -wave pairing are equal here, and almost coincide with the charge density susceptibility ratio. The non-interacting susceptibility for extended  $s$ -wave pairing (and thus  $\chi$ ) is however much smaller than the other two (see Appendix).

Decreasing the density (away from half-filling) one enters a regime where pairing correlations with  $d_{x^2-y^2}$  symmetry dominate at sufficiently low energy scales. This is seen in Fig. 7, where we show the flow for  $t' = 0$  and  $\mu = -0.02$ , corresponding to  $n = 0.984$ . Note that for small  $U$  the transition from antiferromagnetism to superconductivity occurs already at a critical density  $n_c$  quite close to half-filling. For increasing  $U$  the deviation of  $n_c$  from half-filling increases. The flow in Fig. 7 exhibits a threshold at  $\Lambda = 2|\mu|$  below which the amplitudes for various scattering processes, especially umklapp scattering, renormalize only very slowly. The flow of the antiferromagnetic spin susceptibility is cut off at the same scale. The infinite slope singularity in some of the flow curves at scale  $\Lambda = |\mu|$  is due to the van Hove singularity being

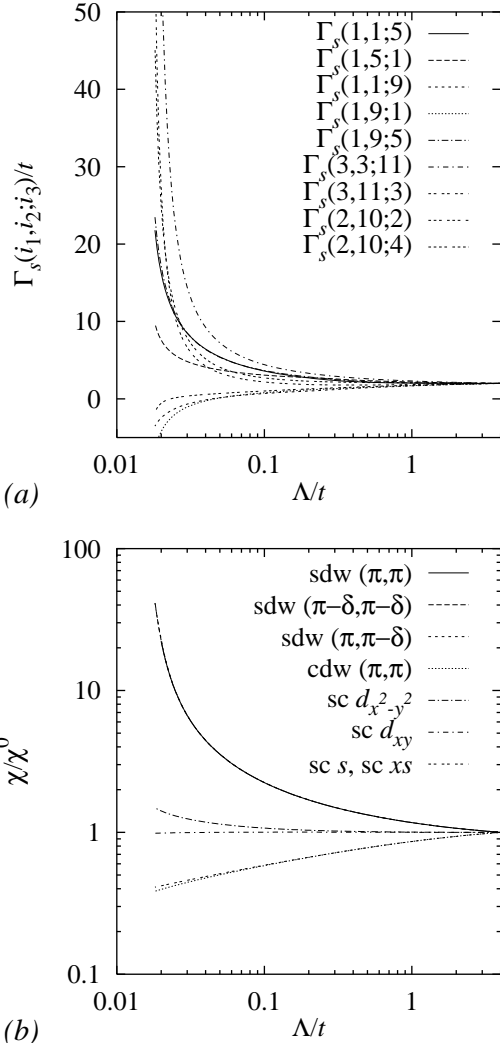


FIG. 6. (a) The flow of the singlet vertex function  $\Gamma_s^{\Lambda}$  as a function of  $\Lambda$  for several choices of the momenta  $\mathbf{k}_{F1}$ ,  $\mathbf{k}_{F2}$  and  $\mathbf{k}'_{F1}$ , which are labelled according to the numbers in Fig. 5. The model parameters are  $U = t$  and  $t' = 0$ , the chemical potential  $\mu = -0.005$ ; (b) the flow of the ratio of interacting and non-interacting susceptibilities,  $\chi^{\Lambda}/\chi_0^{\Lambda}$  for the same system.

crossed at that scale. The pairing susceptibility with  $d_{x^2-y^2}$ -symmetry is obviously dominant here (note the logarithmic scale). Following the flow of the vertex function and susceptibilities one can see that the  $d_{x^2-y^2}$ -pairing correlations develop in the presence of pronounced but *short-range antiferromagnetic spin-correlations*, in agreement with earlier ideas on  $d$ -wave superconductivity [3].

In Fig. 8 we show the  $(\mu, U)$  phase diagram for  $t' = 0$  obtained by identifying the dominant instability from the flow for many different values of  $\mu$  and  $U$ . Note that  $\mu = 0$  corresponds to half-filling. The regime with a leading commensurate antiferromagnetic spin density instability is separated from the  $d$ -wave pairing regime by

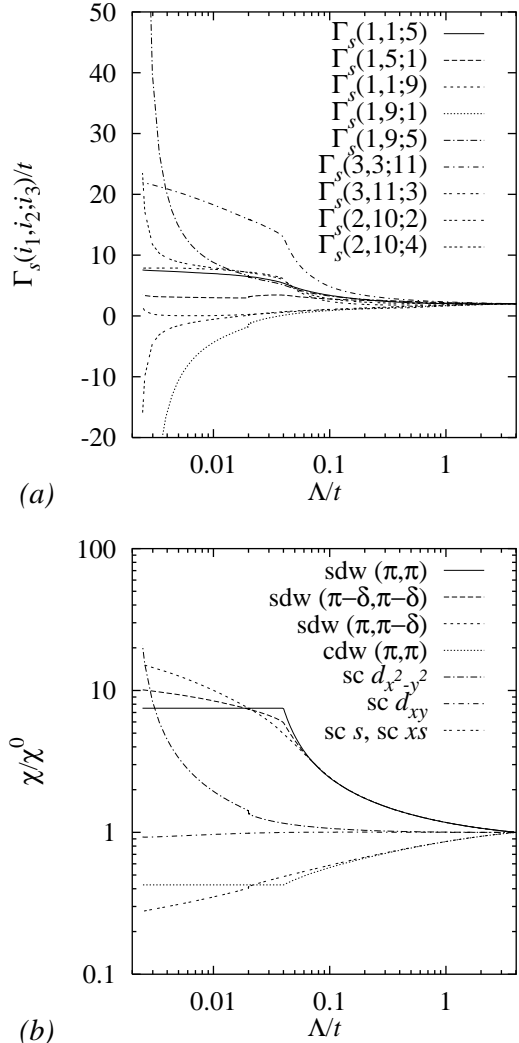


FIG. 7. Same as Fig. 6 for  $U = t$ ,  $t' = 0$  and  $\mu = -0.02$ .

a thin region where incommensurate spin density fluctuations with  $\mathbf{q} = (\pi, \pi - \delta)$  dominate. Other incommensurate structures may be more favorable than the ones considered here. For  $U \rightarrow 0$  at fixed density  $n < 1$  the superconducting instability always dominates, because the bare particle-hole bubbles are finite away from half-filling, while the Cooper channel always diverges at least logarithmically. The way the critical energy scale  $\Lambda_c$  varies as the system is doped away from half-filling can be seen in Fig. 9 for an interaction strength  $U = t$ .

The different symbols show which instability is leading at  $\Lambda_c$ . The two straight lines represent the linear functions  $\Lambda_c = |\mu|$  and  $\Lambda_c = 2|\mu|$ , respectively. As already observed by Zanchi and Schulz [18], the superconducting instability is leading if  $\Lambda_c < |\mu|$ . This may be related to the fact that only pair fluctuations receive a singular enhancement at  $\Lambda = |\mu|$  (see Fig. 7), while spin fluctuations don't. A commensurate spin density wave instability cannot be favorable for  $\Lambda_c < 2|\mu|$ , since their

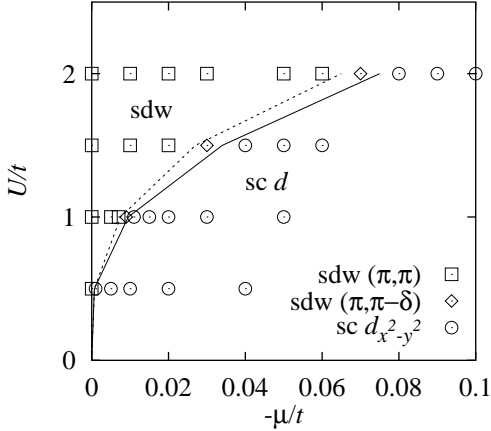


FIG. 8. The  $(\mu, U)$  phase diagram for  $t' = 0$  near half-filling; the symbols represent the parameters for which the flow has been computed; the solid line separates the spin-density wave regime from the superconducting regime, the dotted line separates the commensurate and incommensurate spin-density regions.

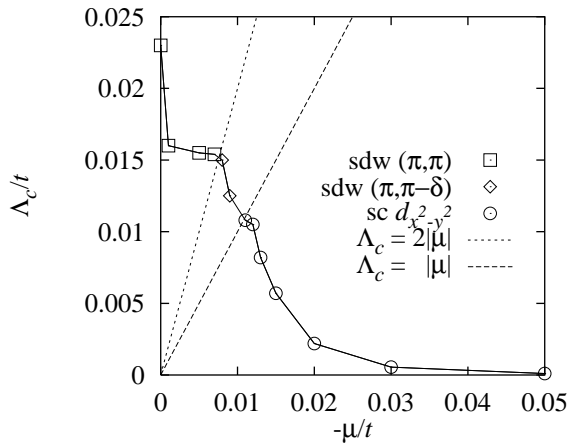


FIG. 9. The critical energy scale  $\Lambda_c$  as a function of the chemical potential  $\mu$  for  $U = t$  and  $t' = 0$ . The different symbols indicate, whether the leading instability is a commensurate or incommensurate spin-density wave or  $d$ -wave pairing instability; the straight lines represent the functions  $\Lambda_c = |\mu|$  and  $\Lambda_c = 2|\mu|$ , respectively.

flow is cut off at  $\Lambda = 2|\mu|$  (see Fig. 7 once again). Hence, the incommensurate spin density wave is the leading for  $|\mu| < \Lambda_c < 2|\mu|$ . The sharp peak in  $\Lambda_c$  at  $\mu = 0$  (half-filling) is due to the van Hove singularity. For larger deviations from half-filling, the critical energy scale  $\Lambda_c$  vanishes rapidly. Note, however, that for larger values of  $U$  the regime with a sizable scale  $\Lambda_c$  extends to larger values of  $\mu$ , i.e. to larger doping.

In Fig. 10 (a) and (b) we show results for the compressibility and the homogeneous spin susceptibility, respectively, for two choices of the chemical potential, at  $U = t$  and  $t' = 0$ . We recall that these quantities have been ob-

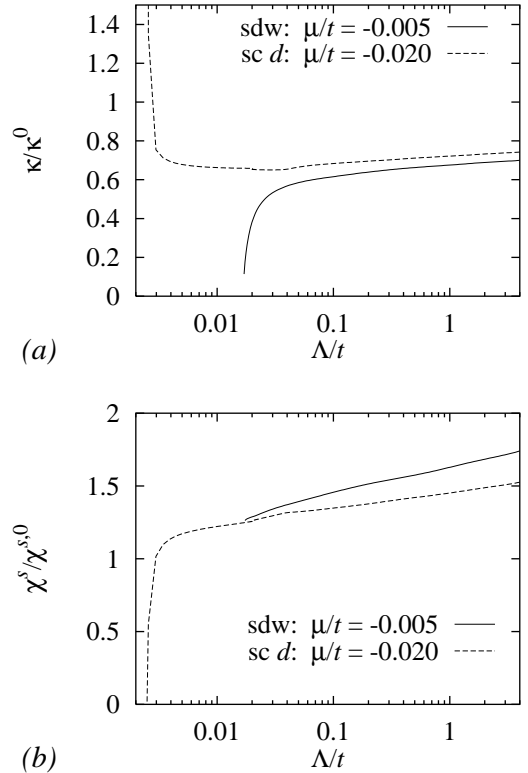
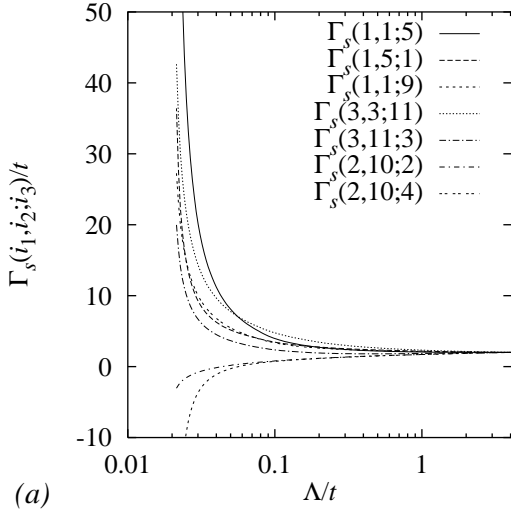
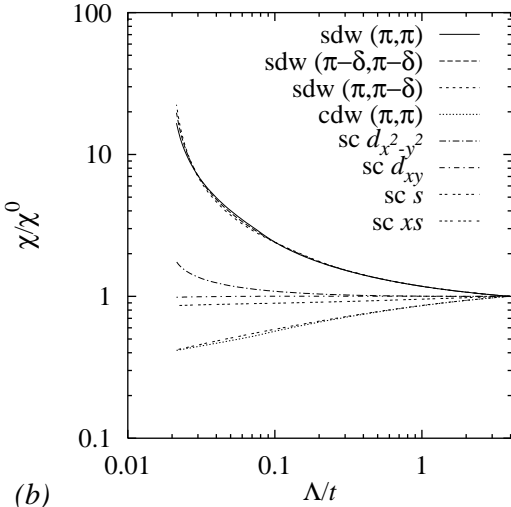


FIG. 10. The flow of (a) the compressibility and (b) the homogeneous spin susceptibility as a function of  $\Lambda$  for various choices of  $\mu$  at  $U = 1$  and  $t' = 0$ ;  $\kappa^0$  and  $\chi^{s,0}$  are the corresponding non-interacting quantities.

tained from the forward scattering vertex by using Fermi liquid relations as discussed above. The non-interacting compressibility  $\kappa^0$  and spin susceptibility  $\chi^{s,0}$  in the plotted ratios are defined without infrared cutoff. Hence the flow in Fig. 10 is entirely due to the flow of the Landau function, starting at the simple RPA result for the Hubbard model at  $\Lambda = \Lambda_0$ . Close to half-filling, where a spin-density wave instability is leading, the compressibility is suppressed at low energy scales, as expected for a system with a charge gap at or near the chemical potential. The homogeneous spin susceptibility remains finite near the spin-density wave instability. By contrast, further away from half-filling in the regime where the  $d$ -wave pairing instability is leading, the compressibility diverges while the homogeneous spin susceptibility is suppressed. A suppressed spin susceptibility is expected as a precursor of the spin gap opening in any spin singlet superconductor. Very close to the instability the spin susceptibility flows through zero to negative values, which implies that our 1-loop calculation breaks down in this strong coupling regime. A diverging compressibility would indicate a tendency towards phase separation, but the increase of  $\kappa$  sets in quite abruptly only very close to the instability, where the renormalized couplings are already so large that the 1-loop results are not reliable any more. In any case the large charge fluctuations indicated by  $\kappa \rightarrow \infty$



(a)

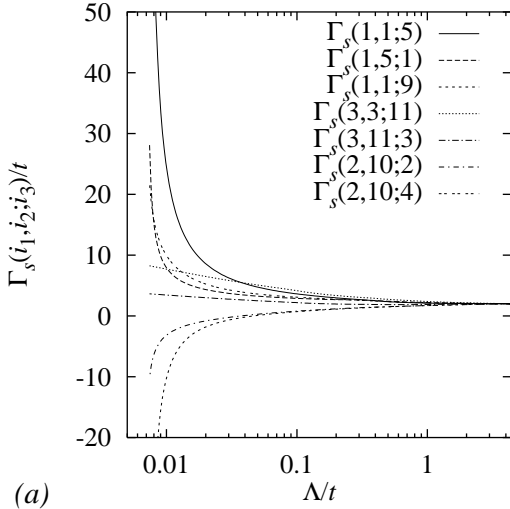


(b)

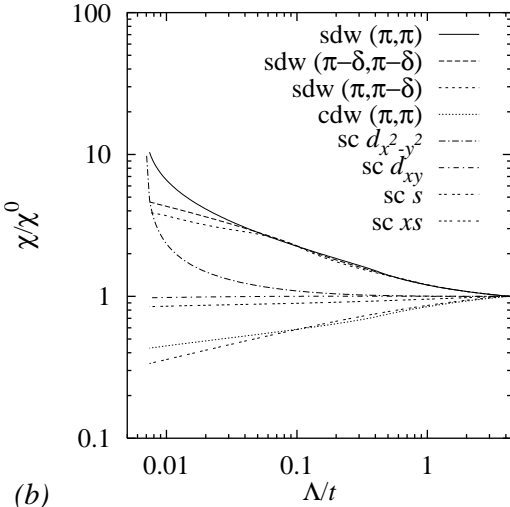
FIG. 11. Same as Fig. 6 for  $U = t$ ,  $t' = -0.01$  and  $\mu = 4t'$ .

would only be a consequence of the pairing instability of the Hubbard model, not a driving mechanism, since the pairing correlations appear already at a higher energy scale.

Results for the flow of the vertex function and susceptibilities for  $t' < 0$  and  $\mu = \epsilon_{vH} = 4t'$  are shown in Figs. 11 and 12, with  $t' = -0.01$  and  $t' = -0.05$ , respectively. The corresponding Fermi surfaces touch the saddle points at  $(\pi, 0)$  and  $(0, \pi)$ . In the first case the density is  $n = 0.992$  and in the second one  $n = 0.959$ . For the bare interaction we have chosen  $U = t$  as before. The major difference with respect to the perfect nesting case  $t' = 0$  is that now the umklapp processes near the diagonal of the Brillouin zone are much less enhanced at low energy scales, such that scattering processes with momenta near the van Hove points  $(\pi, 0)$  and  $(0, \pi)$  become most prominent. In this situation the simple scaling approaches which concentrated exclusively on the van Hove points [10,13] provide already a useful qualitative picture of the important effective interactions and their



(a)



(b)

FIG. 12. Same as Fig. 6 for  $U = t$ ,  $t' = -0.05$  and  $\mu = 4t'$ .

renormalization. Antiferromagnetic correlations are now mostly driven by umklapp processes from  $(\pi, 0)$  to  $(0, \pi)$  and vice versa which, due to the equivalence of the points  $(\pi, 0) = (-\pi, 0)$  and  $(0, \pi) = (0, -\pi)$  in the Brillouin zone, can also be viewed as Cooper processes. Indeed these processes are also responsible for  $d$ -wave pairing correlations.

For the parameters chosen in Fig. 11 antiferromagnetic correlations dominate over pairing. The incommensurate susceptibility with  $\mathbf{q} = (\pi, \pi - \delta)$  is a bit larger than the other incommensurate candidate and the commensurate antiferromagnetic susceptibility. Note that there may be other still larger incommensurate susceptibilities among those not computed here. We have merely investigated two (frequently discussed) incommensurate spin susceptibilities out of a variety of infinitely many candidates. Moving further away from half-filling, as in Fig. 12, one finds again dominant pairing susceptibilities, with  $d_{x^2-y^2}$  symmetry in each case.

The phase diagram in the  $(t', U)$ -plane with  $\mu = 4t' \leq$

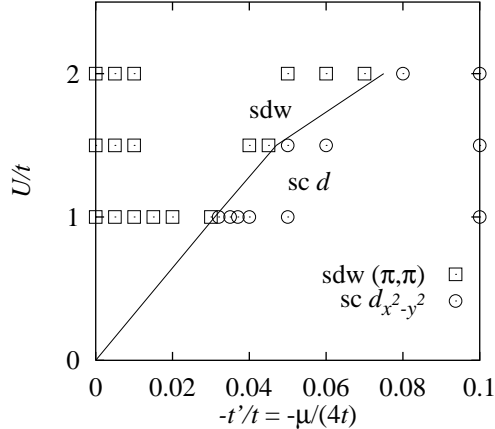


FIG. 13. The  $(t', U)$  phase diagram for  $\mu = 4t' \leq 0$ .

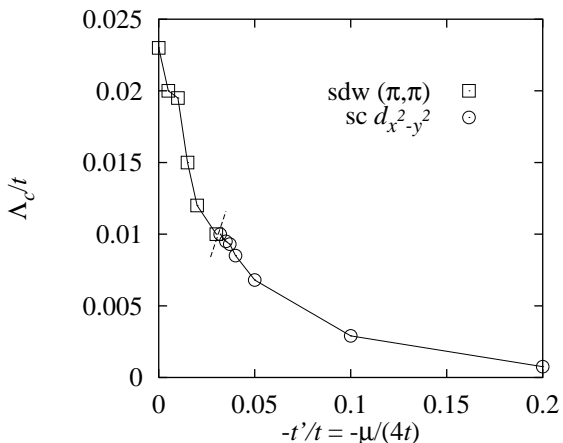


FIG. 14. The critical energy scale  $\Lambda_c$  as a function of  $t'$  for  $\mu = 4t' < 0$  and  $U = t$ ; the short dotted line separates the spin density regime from the  $d$ -wave pairing regime.

0 is shown in Fig. 13. Note that the chemical potential is always situated at the van Hove singularity here and the density decreases away from half-filling with increasing  $|t'|$ . Since we have no good guess for the optimal density dependence of the incommensurability vector for  $t' \neq 0$  we have not distinguished different spin density waves in Fig. 13. The behavior of  $\Lambda_c$  as a function of  $t' < 0$  with  $\mu = 4t'$  and  $U = t$  is shown in Fig. 14.

The decrease of  $\Lambda_c$  with increasing  $|\mu|$  (and thus increasing doping) is slower here than in Fig. 9, since the Fermi level remains on the van Hove singularity such that only the importance of nesting is weakened under doping.

All the numerical results discussed above have been obtained by projecting momentum variables of the vertex function on 16 points on the Fermi surface as shown in Fig. 5. To see how much these results may be modified in a more refined projection scheme, we have computed the flow for some typical model parameters with a projection

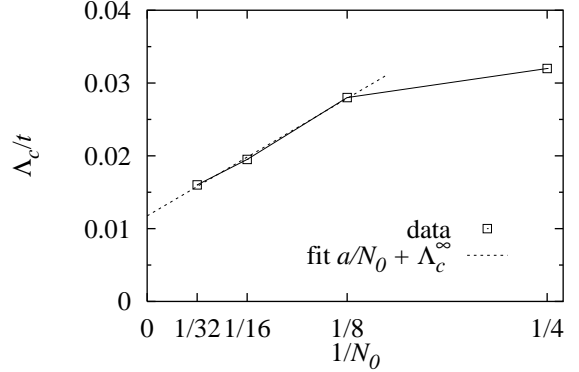


FIG. 15. The critical energy scale  $\Lambda_c$  as a function of the number of discretization points  $N_0$  on the Fermi surface, for  $U = t$ ,  $t' = -0.01t$  and  $\mu = 4t'$ .

on 32 points on the Fermi surface, and also with a projection on 16 Fermi surface points and 16 additional points on the van Hove surface. It turned out that these refinements, which increase the computational effort considerably, lead only to a moderate reduction of the critical energy scale, without changing the qualitative behavior of the vertex function and susceptibilities. In Fig. 15 we show the dependence of the critical scale  $\Lambda_c$  as a function of the inverse number of discretization points  $N_0$  on the Fermi surface for  $N_0 = 4, 8, 16, 32$  and a fixed choice of model parameters. We see that the critical energy scale obtained from a discretization with 16 points has already the right order of magnitude.

#### IV. CONCLUSION

In summary, we have shown that the renormalization group method developed by Salmhofer [20] with our extension for the computation of susceptibilities can be used as a systematic tool for detecting instabilities in a weakly interacting Fermi system with several coupled infrared singularities. Such an RG analysis is completely unbiased. The selection of retained Feynman diagrams is dictated by the weak coupling expansion and can be systematically improved by including higher orders in a loop expansion.

Evaluating the flow equations on 1-loop level for the 2D Hubbard model we have found antiferromagnetic instabilities close to half-filling and dominant superconducting instabilities with  $d_{x^2-y^2}$  symmetry at smaller densities (still near half-filling). Incommensurate spin structures can be favorable in the antiferromagnetic regime near half-filling.

The critical energy scale  $\Lambda_c$  where vertex functions and susceptibilities diverge vanishes exponentially as  $U \rightarrow 0$ , but becomes sizable already for relatively weak coupling strengths (compared to the band width), even in the superconducting regime. The appearance of strong pairing correlations with  $d_{x^2-y^2}$  symmetry in the 2D Hubbard model at physically interesting energy scales is thus

well established at weak coupling. The flow of the vertex function and susceptibilities clearly shows that the pairing instability is driven by short-range antiferromagnetic correlations in the system. This supports earlier ideas and numerical results (for finite systems) suggesting  $d$ -wave superconductivity driven by antiferromagnetic correlations in the Hubbard model [3]. Note that  $\Lambda_c$  must not be interpreted as a transition temperature for antiferromagnetism or superconductivity, but rather as an energy scale where bound particle-particle or particle-hole pairs are formed. A Kosterlitz-Thouless transition to a superconducting state may occur at a lower energy scale while antiferromagnetic order is of course possible only in the ground state of a two dimensional system with spin-rotation invariance.

We finally outline some interesting extensions of the present work for the future:

- i) *Non-local interactions:* Non-local interactions may play an important role even though they are usually much smaller than the local (Hubbard) interaction. They affect the RG flow via a different initial condition for the vertex function and can thus be taken into account very easily.
- ii) *Fermi surface instabilities:* The Fermi surface is generally deformed by interactions. Computing a susceptibility for Fermi surface deformations from the RG flow one finds that deformations breaking the discrete square lattice symmetry may occur [30].
- iii) *Self-energy effects:* It will be interesting to compute self-energy contributions and see how they affect the instabilities. The numerical effort for this is small on 1-loop level, but also a 2-loop calculation seems feasible. Kishine and Yonemitsu [31] have recently computed the renormalization of the quasi-particle weight on 2-loop level for two flat Fermi surface pieces, but the feedback of self-energy effects on instabilities has not yet been treated.

#### Acknowledgments:

We are very grateful to Manfred Salmhofer for explaining to us his renormalization group scheme before publication and giving us several useful hints during the initial stage of this work. We would also like to thank Maurice Rice, Eugene Trubowitz and Victor Yakovenko for valuable discussions. This work has been supported by the Deutsche Forschungsgemeinschaft under Contract No. Me 1255/4-1,2.

#### APPENDIX A: NON-INTERACTING SUSCEPTIBILITIES

Here we show results for the flow of the non-interacting susceptibilities  $\chi_0^\Lambda$  for the choices of  $t'$  and  $\mu$  corresponding to those in Fig. 6, 7, 11 and 12. The reader may thus estimate the absolute scale of  $\chi^\Lambda$  by multiplying  $\chi_0^\Lambda$  with the results for the ratios  $\chi^\Lambda/\chi_0^\Lambda$  in Sec. III.

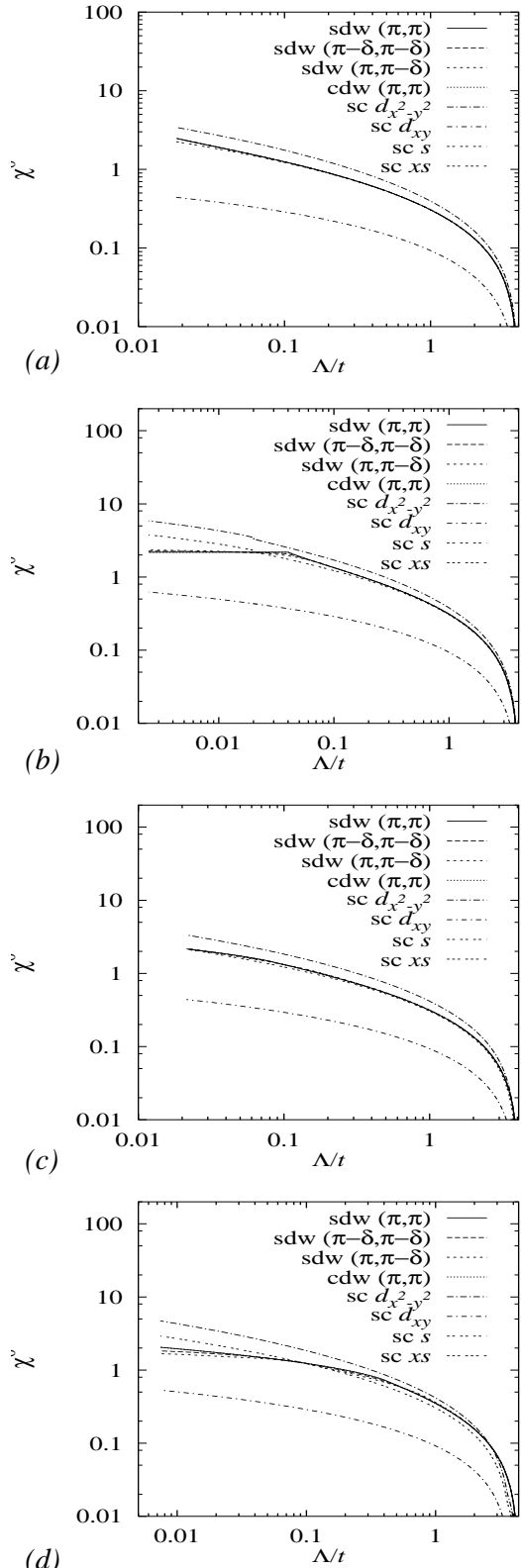


FIG. 16. Free susceptibilities for (a)  $t' = 0$  and  $\mu = -0.005t$ , (b)  $t' = 0$  and  $\mu = -0.02t$ , (c)  $t' = -0.01t$  and  $\mu = 4t'$  and (d) for  $t' = -0.05t$  and  $\mu = 4t'$ , corresponding to the examples in Fig. 6, 7, 11 and 12, respectively.

The incommensurate spin-density susceptibilities and the charge-density susceptibility lie too close together to be always individually seen. The extended  $s$ -wave pairing susceptibility is of the order of  $10^{-4}$  and therefore out of scale.

---

- [1] D. M. Ginsberg (ed.), *Physical Properties of High Temperature Superconductors*, Vol. 1-5 (World Scientific, Singapore).
- [2] See, for example, *The Hubbard Model*, ed. A. Montorsi (World Scientific 1992).
- [3] For a review on  $d$ -wave superconductivity, see D. J. Scalapino, Phys. Rep. **250**, 329 (1995).
- [4] N. E. Bickers, D. J. Scalapino, and S. R. White, Phys. Rev. Lett. **62**, 961 (1989).
- [5] I. T. Diatlov, V. V. Sudakov, and K. A. Ter-Martirosian, Zh. Eksp. Teor. Fiz. **32**, 767 (1957) [Sov. Phys. JETP **5**, 631 (1957)].
- [6] For an early review on 1D Fermi systems, see J. Solyom, Adv. Phys. **28**, 201 (1979).
- [7] For a comprehensive modern review on 1D Fermi systems, see J. Voit, Rep. Prog. Phys. **57**, 977 (1994).
- [8] H. J. Schulz, Europhys. Lett. **4**, 609 (1987).
- [9] I. Dzyaloshinskii, Sov. Phys. JETP **66**, 848 (1987).
- [10] P. Lederer, G. Montambaux, and D. Poilblanc, J. Phys. (Paris) **48**, 1613 (1987).
- [11] J. González, F. Guinea, and M. A. H. Vozmediano, Europhys. Lett. **34**, 711 (1996); Nucl. Phys. B **485**, 694 (1997).
- [12] I. Dzyaloshinskii, J. Phys. I **6**, 119 (1996).
- [13] N. Furukawa, T. M. Rice, and M. Salmhofer, Phys. Rev. Lett. **81**, 3195 (1998).
- [14] A. Houghton and J. B. Marston, Phys. Rev. B **48**, 7790 (1993).
- [15] N. Furukawa and T. M. Rice, J. Phys. Condens. Matter **10**, L381 (1998).
- [16] J. González, F. Guinea, and M. A. H. Vozmediano, Phys. Rev. Lett. **79**, 3514 (1997).
- [17] A. T. Zheleznyak, V. M. Yakovenko, and I. E. Dzyaloshinskii, Phys. Rev. B **55**, 3200 (1997).
- [18] D. Zanchi and H. J. Schulz, Z. Phys. B **103**, 339 (1997); Europhys. Lett. **44**, 235 (1998); cond-mat/9812303.
- [19] J. Polchinski, Nucl. Phys. **B231**, 269 (1984).
- [20] M. Salmhofer, Commun. Math. Phys. **194**, 249 (1998).
- [21] For a short review, see J. Feldman, J. Magnen, V. Rivasseau, and E. Trubowitz, in *The State of Matter*, edited by M. Aizenmann and H. Araki, Advanced Series in Mathematical Physics Vol. 20 (World Scientific 1994).
- [22] J. Feldmann, H. Knörrer, D. Lehmann, and E. Trubowitz in *Constructive Physics*, edited by V. Rivasseau, Springer Lecture Notes in Physics Vol. 446 (Springer 1995); J. Feldmann, M. Salmhofer, and E. Trubowitz, J. Stat. Phys. **84**, 1209 (1996); Commun. Pure Appl. Math. **51**, 1133 (1998); Commun. Pure Appl. Math. **52**, 273 (1999).
- [23] See, for example, J. W. Negele and H. Orland, *Quantum Many-Particle Systems* (Addison-Wesley, 1987).
- [24] M. Salmhofer, *Renormalization* (Springer 1998).
- [25] D. C. Brydges and J. Wright, J. Stat. Phys. **51**, 435 (1988).
- [26] See, for example, R. Shankar, Rev. Mod. Phys. **66**, 129 (1994).
- [27] For the relation between RG and Fermi liquid theory see, for example, W. Metzner, C. Castellani and C. Di Castro, Adv. Phys. **47**, No. 3 (1998).
- [28] D. Pines and P. Nozières, *The Theory of Quantum Liquids* (Benjamin 1966).
- [29] See, for example, H. J. Schulz, Phys. Rev. Lett. **64**, 1445 (1990), where also the choice of  $\delta$  as a function of doping is discussed.
- [30] C. J. Halboth and W. Metzner, in preparation.
- [31] J. Kishine and K. Yonemitsu, Phys. Rev. B **59**, 14823 (1999).